

Roles of Arginine and Lysine Residues in the Translocation of a Cell-Penetrating Peptide from ^{13}C , ^{31}P , and ^{19}F Solid-State NMR[†]

Yongchao Su,[‡] Tim Doherty,[‡] Alan J. Waring,[§] Piotr Ruchala,^{||} and Mei Hong^{*‡}

[‡]Department of Chemistry, Iowa State University, Ames, Iowa 50011, [§]Department of Medicine, David Geffen School of Medicine, University of California, Los Angeles, California 90095, and ^{||}David Geffen School of Medicine, University of California, 10833 Le Conte Avenue, CHS 37-068, Los Angeles, California 90095

Received January 20, 2009; Revised Manuscript Received April 11, 2009

ABSTRACT: Cell-penetrating peptides (CPPs) are small cationic peptides that cross the cell membrane while carrying macromolecular cargoes. We use solid-state NMR to investigate the structure and lipid interaction of two cationic residues, Arg₁₀ and Lys₁₃, in the CPP penetratin. ^{13}C chemical shifts indicate that Arg₁₀ adopts a rigid β -strand conformation in the liquid-crystalline state of anionic lipid membranes. This behavior contrasts with all other residues observed so far in this peptide, which adopt a dynamic β -turn conformation with coil-like chemical shifts at physiological temperature. Low-temperature ^{13}C – ^{31}P distances between the peptide and the lipid phosphates indicate that both the Arg₁₀ guanidinium C ζ atom and the Lys₁₃ C ϵ atom are close to the lipid ^{31}P (4.0–4.2 Å), proving the existence of charge–charge interaction for both Arg₁₀ and Lys₁₃ in the gel-phase membrane. However, since lysine substitution in CPPs is known to weaken their translocation ability, we propose that the low temperature stabilizes interactions of both lysine and arginine with the phosphates, whereas at high temperatures, the lysine–phosphate interaction is much weaker than the arginine–phosphate interaction. This is supported by the unusually high rigidity of the Arg₁₀ side chain and its β -strand conformation at high temperatures. The latter is proposed to be important for ion pair formation by allowing close approach of the lipid headgroups to guanidinium side chains. ^{19}F and ^{13}C spin diffusion experiments indicate that penetratin is oligomerized into β -sheets in gel-phase membranes. These solid-state NMR data indicate that guanidinium–phosphate interactions exist in penetratin, and guanidinium groups play a stronger structural role than ammonium groups in the lipid-assisted translocation of CPPs across liquid-crystalline cell membranes.

Cell-penetrating peptides (CPP) are arginine- and lysine-rich cationic peptides that can readily enter cells not only by themselves but also carrying other macromolecular cargoes (1–3). Thus, they are promising drug-delivery molecules. Many studies have established that the intracellular entry of CPPs is related to their strong affinity for lipid bilayers (4). The lipid membrane can be the plasma membrane of the cell or the endosomal membrane from which CPPs must escape after endocytosis (5). The fundamental biophysical question of interest is how these highly cationic peptides cross the hydrophobic part of the lipid bilayer against the free energy barrier and do so without causing permanent damage to the membrane, in contrast to another family of cationic membrane peptides, antimicrobial peptides (AMPs).

Several models for explaining the membrane translocation of CPPs have been proposed. The inverse micelle model proposes that transient inverse micelles form in the membrane to trap the peptides from the outer leaflet and subsequently release them to

the inner leaflet (6, 7). However, this model is inconsistent with the lipid ^{31}P spectra (8), and the large rearrangement of lipids is difficult to achieve energetically. The electroporation model (9) posits that at low concentrations CPPs bind only to the outer leaflet of the bilayer, thus causing a transmembrane electric field. Above a threshold peptide concentration, the membrane is permeabilized in an electroporation-like manner, which creates transient defects that enable the peptides to distribute to both leaflets, thus relieving the membrane curvature stress (9–11). The third model posits that the guanidinium ions in these arginine-rich peptides associate with the lipid phosphate groups to neutralize the arginine residues and thus allow the peptides to cross the membrane without a high energy penalty. This model is supported by phase transfer experiments with oligoarginines (12) and by molecular dynamics simulation of the HIV-1 Tat peptide, which showed transient association of arginine residues with the phosphate groups on both sides of the bilayer (13).

We recently investigated the depth of insertion and conformation of a CPP, penetratin, using solid-state ^{13}C and ^{31}P NMR. Penetratin is the first discovered CPP and is derived from the third helix (residues 43–58) of the *Drosophila Antennapedia* homeodomain (14). Using Mn^{2+} paramagnetic relaxation enhancement (PRE) experiments, we showed that penetratin is

[†]This work is supported by National Institutes of Health Grant GM-066976 to M.H.

*To whom correspondence should be addressed: Department of Chemistry, Iowa State University, Ames, IA 50011. Telephone: (515) 294-3521. Fax: (515) 294-0105. E-mail: mhong@iastate.edu.

bound to both leaflets of the lipid bilayer at both low and high concentrations (peptide:lipid molar ratios of 1:40 and 1:15) (15, 16). These data indicate that the electroporation model is unlikely for penetratin. No ^{31}P peaks at the isotropic frequency or the hexagonal-phase frequency were observed, thus ruling out the inverse micelle model. In addition, we found that penetratin undergoes an interesting conformational change, as manifested by ^{13}C chemical shifts, from a β -sheet structure in the gel-phase membrane to a coil-like conformation in the liquid-crystalline membrane (17). The coil-like conformation at high temperatures has non-negligible residual order parameters of 0.23–0.52 (17), indicating that the peptide remains structured. We hypothesized that the high-temperature conformation is a β -turn that undergoes uniaxial rotation around the bilayer normal.

Given the experimental evidence against the electroporation model and the inverse micelle model described above, we now test the validity of the guanidinium phosphate complexation model for the membrane translocation of penetratin. For this purpose, we measured ^{13}C – ^{31}P distances between several peptide side chains and lipid ^{31}P atoms. As shown before for an arginine-rich antimicrobial peptide, strong associations with the lipid phosphates manifest as short ^{13}C – ^{31}P distances (18, 19). We show here that the cationic Arg₁₀ in penetratin indeed exhibits shorter distances to phosphate groups than hydrophobic residues. However, another cationic residue, Lys₁₃, also exhibits short ^{13}C – ^{31}P distances, despite the fact that Lys mutants of CPPs have much weaker translocation activities. We show that the answer to this puzzle lies not in the low-temperature structure and distances of the two residues, but in their high-temperature dynamic structures, which differ significantly. And it is the structure in the liquid-crystalline membrane that accounts for the distinct roles of Arg and Lys in entry of CPP into the cell. Finally, we investigate the oligomeric structure of penetratin in gel-phase membranes using ^{19}F and ^{13}C spin diffusion NMR.

MATERIALS AND METHODS

All lipids were purchased from Avanti Polar Lipids (Alabaster, AL) and used without further purification. Penetratin (RQIKI WFQNR RMKW KK), which contains three arginines and four lysines, was synthesized using standard Fmoc solid-phase peptide synthesis methods (20). Uniformly ^{13}C - and ^{15}N -labeled arginine was purchased from Cambridge Isotope Laboratory and incorporated into Arg₁₀ in the peptide. Ile₃ and Lys₁₃ were labeled in two other peptide samples as described previously (17). 4- ^{19}F -Phe₇ labeled penetratin was used for ^{19}F experiments to determine the oligomeric structure. All peptide samples were purified by HPLC to >95% purity.

Hydrated membrane samples were prepared using an aqueous-phase mixing method. Lipids were first codissolved in chloroform at the desired molar ratios and dried under a stream of N_2 gas. After lyophilization in cyclohexane overnight, the dry lipid powder was suspended in water and frozen and thawed several times before the peptide solution was added. The solution was incubated overnight to facilitate binding and then centrifuged at 55000 rpm for 3 h to yield a hydrated membrane pellet. For the Arg₁₀ experiments, a hydrated DMPC/DMPG¹ (8:7) membrane

with a peptide:lipid molar ratio of 1:15 was used in most two-dimensional (2D) correlation and distance measurements. The molar ratio was chosen to balance the positive charges of the peptide (+7) with the negatively charged PG lipids (−1). This DMPC/DMPG sample was supplemented with a hydrated POPC/POPG (8:7) sample for the conformation study, and with a trehalose-protected dry POPE/POPG (8:7) sample for the ^{13}C – ^{31}P REDOR experiment. For distance measurements of other residues, several trehalose-protected dry DMPC/DMPG membranes were used to ensure that both the peptide and the lipid headgroups were completely immobilized at low temperatures (21). Trehalose is known to protect the lamellar structure of the lipid bilayer in the absence of water (22). Below we refer to the non-trehalose-containing membrane samples as hydrated samples to distinguish them from the dry trehalose-containing samples.

Solid-State NMR Experiments. All experiments were conducted on a Bruker (Karlsruhe, Germany) DSX-400 (9.4 T) spectrometer at a resonance frequency of 100.7 MHz for ^{13}C , 376.8 MHz for ^{19}F , and 162.1 MHz for ^{31}P . Magic-angle-spinning (MAS) probes tuned to $^1\text{H}/^{13}\text{C}/^{31}\text{P}$ and $^1\text{H}/^{19}\text{F}/\text{X}$ and equipped with 4 mm spinning modules were used for all experiments. Low temperatures were achieved using a Kinetics Thermal System (Stone Ridge, NY) XR air-jet sample cooler. The temperature of the sample was read from a thermocouple placed near the rotor and was not further calibrated. Typical 90° pulse lengths are 3.5–5.0 μs . ^1H decoupling fields of 50–80 kHz were used. ^{13}C , ^{31}P , and ^{19}F chemical shifts were referenced externally to the α -Gly ^{13}C ' resonance at 176.49 ppm on the TMS scale, the hydroxyapatite ^{31}P signal at 2.73 ppm, and the Teflon ^{19}F signal at −122 ppm, respectively.

^{13}C cross-polarization (CP) MAS experiments were conducted with a contact time of 0.5–1.0 ms at a typical Hartman–Hahn field strength of 50 kHz. For variable-temperature experiments, samples were stabilized for at least 20 min at each temperature before data were acquired. 2D ^{13}C – ^{13}C dipolar assisted rotational resonance (DARR) experiments (23) were conducted under 5 kHz MAS with mixing times of 20 and 30 ms. A ^1H -driven spin diffusion experiment with a longer mixing time of 50 ms was used to detect inter-residue cross-peaks of penetratin in DMPC/DMPG membranes.

^{13}C – ^1H and ^{15}N – ^1H dipolar couplings were measured using DIPSHIFT (24, 25) experiments at 303 K under 3.401 and 3.000 kHz MAS, respectively. The MREV-8 sequence was used for ^1H homonuclear decoupling (26), with a 105° ^1H pulse length of 4.0 μs . In the C–H DIPSHIFT experiment, the ^{13}C – ^{13}C dipolar coupling is removed by MAS while the ^{13}C – ^{13}C scalar coupling has no effect on the t_1 -dependent intensity modulation due to the constant-time nature of the evolution period. The normalized t_1 intensities were fitted using a home-written Fortran program. The best-fit values were divided by the theoretical scaling factor of 0.47 for the MREV-8 sequence. For the doubled N–H DIPSHIFT experiment, the fit value was further divided by 2 to yield the true couplings. The ratio between the true coupling and the rigid limit value gives the order parameter S_{XH} . The rigid-limit coupling used was 22.7 kHz for C–H and 10.6 kHz for N–H dipolar couplings. Simulations took into account the difference between the XH and XH₂ spin systems.

Frequency selective rotational-echo double-resonance (REDOR) experiments were used to measure distances between peptide ^{13}C and lipid ^{31}P (27, 28). The experiments were conducted at ~230 K under 4 kHz MAS. A rotor-synchronized

¹Abbreviations: DMPC, 1,2-dimyristoyl-*sn*-glycero-3-phosphatidylcholine; DMPG, 1,2-dimyristoyl-*sn*-glycero-3-phosphatidylglycerol; POPC, 1-palmitoyl-2-oleoyl-*sn*-glycero-3-phosphatidylcholine; POPE, 1-palmitoyl-2-oleoyl-*sn*-glycero-3-phosphoethanolamine; POPG, 1-palmitoyl-2-oleoyl-*sn*-glycero-3-phosphatidylglycerol.

soft ^{13}C Gaussian 180° pulse of $1000\ \mu\text{s}$ was applied in the middle of the REDOR period to suppress the ^{13}C – ^{13}C J coupling between the on-resonance ^{13}C and its directly bonded ^{13}C spins. ^{31}P 180° pulses of $9\ \mu\text{s}$ were applied every half-rotor period. The DMPC/DMPG sample was used to measure the distances from the Arg₁₀ side chain and CO to ^{31}P , whereas the POPE/POPG sample was used to measure the C α – ^{31}P distance, as the DMPC C γ peak (54 ppm) overlaps with the Arg₁₀ C α signal.

A double-quantum (DQ) selective REDOR experiment (Figure 5a) was designed to measure the ^{13}C – ^{31}P distance of Ile₃ side chains, whose signals overlap extensively with the lipid ^{13}C peaks. An SPC-5 pulse train (29) was used to create DQ coherence of the labeled ^{13}C sites and suppress the natural abundance lipid ^{13}C signals. The efficiency of the DQ-REDOR experiment is $\sim 20\%$ of that of the single-quantum selective REDOR experiment.

For the ^{13}CO – ^{31}P REDOR experiment, the DQ-REDOR experiment was not used due to the low sensitivity of the CO signal. Thus, the lipid natural abundance contribution to the ^{13}CO signal was corrected using the equation $(S/S_0)_{\text{observed}} = 0.79(S/S_0)_{\text{peptide}} + 0.21(S/S_0)_{\text{lipid}}$, where the weight fractions were obtained from the peptide:lipid molar ratio. At the low temperature used for the REDOR experiments, the lipid and peptide CO groups have very similar CP efficiencies; thus, the natural abundance correction is relatively accurate.

All ^{13}C – ^{31}P REDOR data were fit by two-spin simulations. As we showed before, for distances shorter than $5\ \text{\AA}$, two-spin simulations are sufficient. For distances greater than $7\ \text{\AA}$, the two-spin simulation only slightly overestimates the distances compared to the vertical distance from ^{13}C to the ^{31}P plane obtained from a multi-spin simulation (18).

The oligomeric structure of penetratin was determined using a ^{19}F CODEX experiment (30, 31). The experiments were conducted at 233 K on a trehalose-protected DMPC/DMPG sample to freeze potential motion of the peptide. Two experiments were conducted for each mixing time: an exchange experiment (S) with the desired mixing time (τ_m) and a short z -filter (τ_z) and a reference experiment (S_0) with interchanged τ_m and τ_z . The normalized intensity, S/S_0 , was measured as a function of the mixing time until it reached a plateau. The inverse of the equilibrium S/S_0 value gives the minimum oligomeric number. Error bars were propagated from the signal-to-noise ratios of the isotropic peak and its sidebands. The τ_m -dependent CODEX curve was simulated as described previously (32) to extract intermolecular distances.

RESULTS

Arg₁₀ Conformation and Dynamics in Penetratin. In this study, we focus on Arg₁₀, one of the three arginine residues in penetratin, to understand whether cationic residues in general and arginine residues in particular play a special role in the membrane translocation of the peptide. We first investigate the conformation of Arg₁₀. We recently reported the reversible conformational change of many penetratin residues in the lipid bilayer between a β -turn state at high temperatures and a β -strand state at low temperatures. This conformational change was manifested as chemical shift changes and was observed at Ile₃, Ile₅, Gln₈, Asn₉, and Lys₁₃. The chemical shift change is independent of the membrane composition (POPC/POPG and DMPC/DMPG), anionic lipid fraction (8:7 and 3:1 PC:PG), and peptide concentration (1:15 and 1:30 P:L) (17).

Figure 1a shows the 2D ^{13}C – ^{13}C correlation spectra of Arg₁₀-labeled penetratin in DMPC/DMPG bilayers at 303 and 234 K. Most intrasidue cross-peaks are seen and show no frequency differences between high and low temperatures. Thus, in contrast to all other residues examined, Arg₁₀ does not have temperature-induced conformational changes. The difference in the experimental isotropic chemical shifts from the random coil values reflects the secondary structure of the protein (33). On the basis of the ^{13}CO , $^{13}\text{C}\alpha$, and $^{13}\text{C}\beta$ ^{13}C isotropic shifts (Table S1 of the Supporting Information), we find Arg₁₀ adopts β -strand conformation at both high and low temperatures.

One-dimensional (1D) ^{13}C CP-MAS spectra scanned between 303 and 233 K (Figure 1b) confirm the lack of chemical shift changes in DMPC/DMPG bilayers. Moreover, the 1D spectra show that the penetratin ^{13}C lines are broader at low temperatures. This phenomenon is common to many membrane peptides (34, 35) and can be attributed to the conformational distribution of the peptide in the lipid membrane, which is averaged at high temperatures but frozen at low temperatures. For the side chain C δ signal, the largest line broadening is observed between 288 and 263 K, below which the lines are sharpened again. This is a definitive signature of intermediate-time scale motion, which means that at 303 K the Arg₁₀ side chain undergoes fast torsional motion. The lack of exchange broadening for the C α and CO signals indicates that the Arg₁₀ backbone is already in the slow motional limit at 303 K.

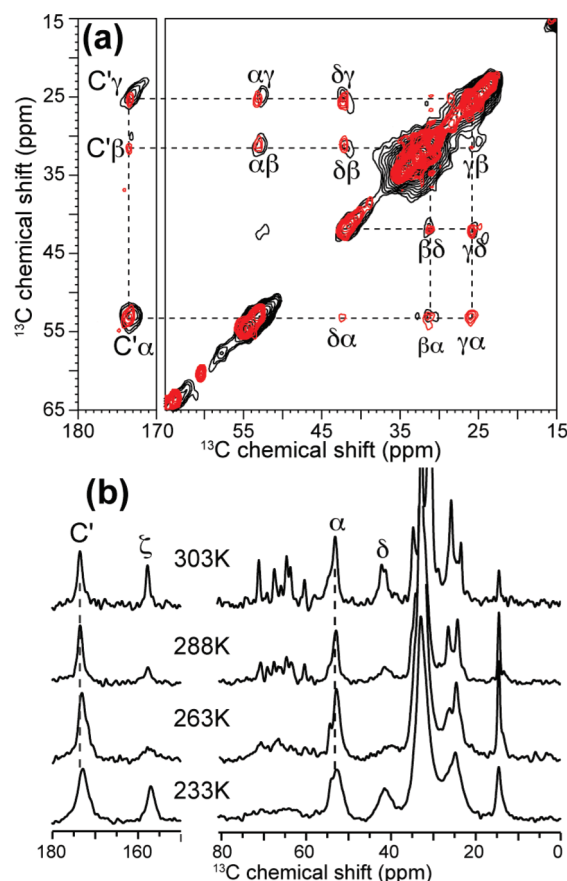


FIGURE 1: (a) 2D ^{13}C – ^{13}C correlation spectra of Arg₁₀-labeled penetratin in DMPC/DMPG (8:7) membranes at 303 (red) and 234 K (black), with DARR mixing times of 30 and 20 ms, respectively. (b) One-dimensional ^{13}C CP-MAS spectra of Arg₁₀-labeled penetratin in the DMPC/DMPG membrane as a function of temperature. Lines guide the eye for Arg₁₀ backbone signals and the lack of temperature-induced chemical shift changes.

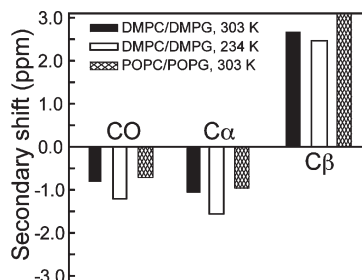


FIGURE 2: ^{13}C secondary chemical shifts of CO, C α , and C β of Arg $_{10}$ of penetratin in two lipid membranes and at two temperatures.

We also measured the Arg $_{10}$ chemical shifts in POPC/POPG (8:7) membranes (Figure S1 of the Supporting Information) and similarly found only β -strand chemical shifts over a wide temperature range. Figure 2 plots the ^{13}C secondary chemical shifts of Arg $_{10}$ at two temperatures in two different lipid membranes. The temperature-independent β -strand conformation of Arg $_{10}$ differs from those of all other residues examined so far in penetratin (17).

The β -strand conformation is usually more rigid than a coil or turn conformation due to hydrogen bond constraints and thus should have order parameters close to 1 (17, 36). To verify this, we measured the C–H dipolar couplings of various Arg $_{10}$ segments in DMPC/DMPG bilayers. Figure 3a shows the ^{13}C – ^1H DIPSHIFT curves of C α and C δ at 303 K. The backbone C α –H α dipolar coupling is 20.9 kHz, corresponding to an S_{CH} of 0.92, which translates to a small motional amplitude of 13° (37). This order parameter fits into the S_{CH} range of 0.89–0.94 measured for the other five residues when they are in

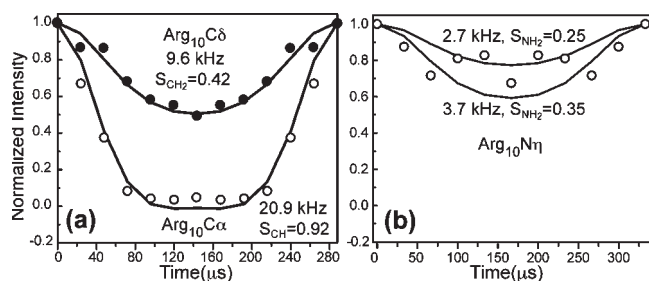


FIGURE 3: X–H DIPSHIFT time evolution of Arg $_{10}$ sites. (a) C–H dipolar couplings of C α (○) and C δ (●) at 303 K, measured under 3.401 kHz MAS. The best-fit true couplings are given along with the corresponding order parameters. (b) N–H dipolar coupling of N η , measured under 3.000 kHz MAS. The scatter in the data is bracketed by two simulated curves, giving an S_{NH} value of 0.30 ± 0.05 .

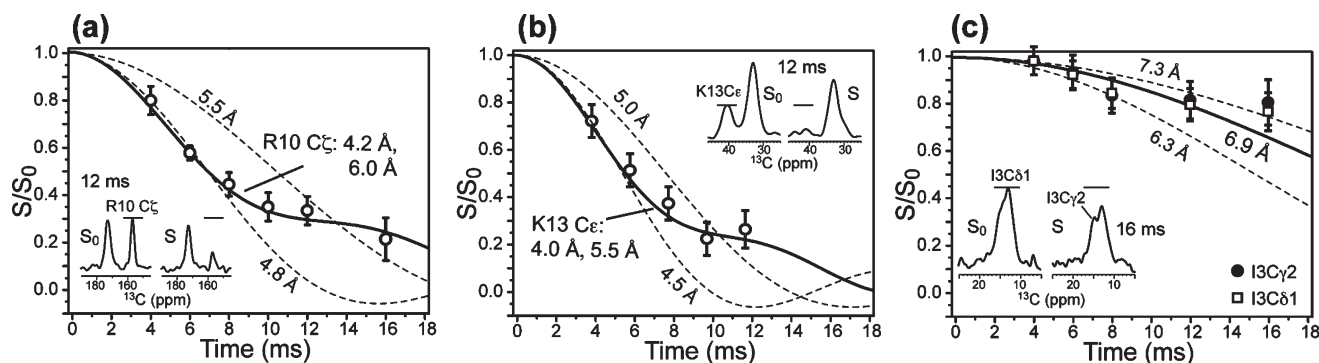


FIGURE 4: ^{13}C – ^{31}P REDOR data of penetratin side chains in lipid membranes at 233 K. (a) Arg $_{10}$ C ζ in hydrated DMPC/DMPG (8:7) bilayers. (b) Lys $_{13}$ C ϵ in dry trehalose-protected DMPC/DMPG (8:7) bilayers. (c) Ile $_3$ methyl groups in dry trehalose-protected DMPC/DMPG (8:7) bilayers. Representative REDOR S_0 and S spectra are shown in the insets.

the β -strand conformation. In comparison, the side chain C δ group has an S_{CH} of 0.42. While this value is much lower than that of the backbone due to the many torsional motions of the side chain, it is actually larger than all other measured side chain order parameters, which range from 0.23 to 0.37 in the β -sheet conformation (17). For the sake of comparison, the Lys $_{13}$ side chain C ϵ group was previously found to have an S_{CH} order parameter of 0.33 (17). We also measured the N–H dipolar coupling of the guanidinium N η group and found an N–H dipolar coupling of 3.2 ± 0.5 kHz (Figure 3b). This translates to an S_{NH} of 0.30 ± 0.05 , which is significant considering this segment is six bonds from the backbone C α group.

^{13}C – ^{31}P Distances between Penetratin and Lipid Headgroups. The main goal of this study is to determine if the cationic residues in penetratin interact strongly with the negatively charged lipid phosphates. ^{13}C – ^{31}P distance measurements can provide this information site-specifically. Figure 4 shows the ^{13}C – ^{31}P REDOR data of Arg $_{10}$, Lys $_{13}$, and Ile $_3$ side chains in DMPC/DMPG membranes. The experiments were conducted at 233 K where the ^{31}P chemical shift span is 195–198 ppm, corresponding to fully immobilized headgroups. The arginine C ζ and lysine C ϵ groups directly neighbor the cationic amines and have well-resolved chemical shifts of 157.0 and 40.2 ppm, respectively; thus, they are ideal reporters of the interaction of these side chain ends with the lipid headgroups. The Arg $_{10}$ C ζ group exhibits significant ^{13}C – ^{31}P REDOR dephasing with an S/S_0 of 0.35 by 10 ms (Figure 4a), indicating relatively short distances to ^{31}P . The time dependence of the REDOR intensities cannot be fit to a single distance due to the presence of a kink around 12 ms. Instead, a combination of a long distance of 6.0 Å and a short distance of 4.2 Å at a 1:1 ratio is found by a least-squares analysis to fit the data best [root-mean-square deviation (rmsd) = 0.029]. The short distance of 4.2 Å can be satisfied only if the guanidinium N–H groups are within hydrogen bonding distance of the O–P groups (18). Similarly, the Lys $_{13}$ C ϵ group exhibits significant dephasing, and the REDOR intensities are best fit by two distances of 4.0 and 5.5 Å (1:1) (rmsd = 0.036). Again, the short distance supports hydrogen bonding with the lipid phosphate groups. Details of the two-distance best fit for Arg $_{10}$ and Lys $_{13}$ are given in Figure S2 of the Supporting Information. Single-distance fitting of the Arg $_{10}$ REDOR data indicates that the longer distance must be greater than 5.5 Å while the shorter distance must be smaller than 4.8 Å (Figure 4a). Further, the ^{13}C – ^{31}P distances cannot be shorter than 3.6 Å due to steric constraints. Thus, two-distance REDOR curves were

calculated using short distances of 3.6–4.8 Å with an increment of 0.2 Å and long distances of 5.4–7.2 Å with an increment of 0.3 Å, and the two contributions were averaged at a 1:1 ratio. The Lys₁₃ data were analyzed similarly. The simulations indicate that the experimental uncertainties for these ^{13}C – ^{31}P REDOR data are approximately ± 0.2 Å for distances shorter than 5.5 Å and ± 0.4 Å for distances longer than 5.5 Å.

Are the short ^{13}C – ^{31}P distances of Arg₁₀ and Lys₁₃ specific to the cationic side chains, or are they also true for hydrophobic residues in penetratin? To answer this question, we measured the $^{13}\text{C}\gamma 2$ – ^{31}P and $^{13}\text{C}\delta 1$ – ^{31}P distances of the neutral hydrophobic residue Ile₃. Its C $\delta 1$ group is three bonds from C α , which is similarly separated from the backbone as lysine C ϵ . To remove the lipid natural abundance ^{13}C signals that overlap with the Ile C $\gamma 2$ and C $\delta 1$ peaks between 8.9 and 19.0 ppm, we designed a DQ selective REDOR experiment, whose pulse sequence is shown in Figure 5a. The DQ-selected spectra of Ile₃ C $\gamma 2$ and C $\delta 1$ signals are shown in Figure 5b (middle and bottom spectra). The REDOR dephasing of Ile₃ is shown in Figure 4c. Much less REDOR decay is observed, with S/S_0 values of ~ 0.80 at 16 ms. The data are best fit to a distance of 6.9 Å for both C $\gamma 2$ and C $\delta 1$, which is 2.7–2.9 Å longer than the Arg₁₀ C ζ and Lys₁₃ C ϵ distances. Thus, the short ^{13}C – ^{31}P distances are specific to arginine and lysine side chains instead of being true for all side chains.

We also measured the ^{13}C – ^{31}P distances of the Arg₁₀ backbone C α and CO groups, which are 6.8 and 7.8 Å, respectively (Figure 6). These values fall into the range of 6.9–8.2 Å previously measured for other residues (15). The ^{13}CO data were corrected for the lipid natural abundance signals, whose systematic uncertainty is much smaller than the random noise of the data. All ^{13}C – ^{31}P distances are summarized in Table 1.

Oligomeric Structure of Penetratin in the Lipid Membrane. The ^{19}F CODEX experiment was used to determine the oligomeric number and intermolecular distances of penetratin in gel-phase membranes. Figure 7a shows the normalized exchange intensities of 4- ^{19}F -Phe₇ penetratin in trehalose-protected DMPC/DMPG bilayers. The CODEX intensities decay to an equilibrium value of 0.35 by 2.5 s, indicating three-spin clusters that can be detected by the ^{19}F distance ruler. To fit the decay trajectory quantitatively, we first assumed an equilateral triangle geometry for the three ^{19}F spins (Figure 7b). The best fit possible under this assumption gives an internuclear distance of 9.0 Å for each side of the triangle; however, the fit curve (dashed line) does not capture the fast initial decay of the experimental data. To better fit the biexponential nature of the data, we then used a triangular geometry with one short distance of much less than 9 Å and two distances longer than or comparable to 9 Å. Modeling of penetratin as a trimer of antiparallel β -strands (see below) yielded one distance of 6.0 Å and two distances of ~ 10 Å (Figure 7c), which were found to give excellent fit to the experimental data.

To further constrain the intermolecular packing of penetratin in the lipid membrane, we measured a 2D ^1H -driven ^{13}C spin diffusion spectrum with a mixing time of 50 ms. Figure 8 shows the 2D spectrum of Ile₅, Gln₈, and Lys₁₃-labeled penetratin in DMPC/DMPG bilayers at 249 K. Two inter-residue cross-peaks were observed: I5 α –K13 α and Q8 δ –I5 α . Since the peptide adopts a β -strand conformation at this temperature, the intramolecular distances are ~ 27 and 11 Å for the I5 α –K13 α and Q8 δ –I5 α cross-peaks, respectively, which are too long to be observed by ^{13}C spin diffusion NMR. Thus, these cross-peaks must result from intermolecular contacts, which are most likely less than 6 Å for the 50 ms mixing time used.

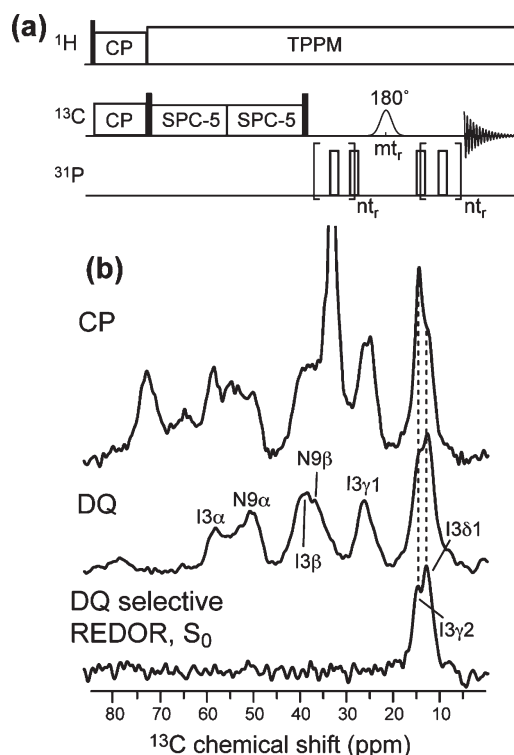


FIGURE 5: (a) Pulse sequence for the DQ selective REDOR experiment. (b) ^{13}C MAS spectra of Ile₃- and Asn₉-labeled penetratin in trehalose-protected DMPC/DMPG bilayers: (top) CP spectrum, showing both the lipid and peptide signals, (middle) DQ-filtered spectrum, showing only peptide signals, and (bottom) DQ selective REDOR S_0 spectrum, showing only the Ile₃ side chain C $\gamma 2$ and C $\delta 1$ signals.

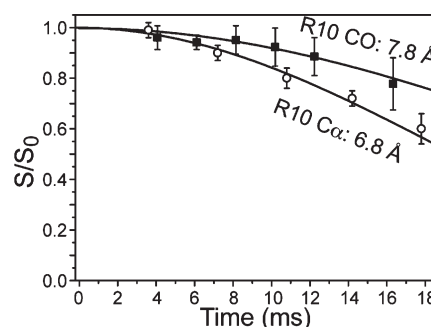


FIGURE 6: ^{13}C – ^{31}P REDOR of Arg₁₀ C α (O) and CO (●) at 233 K. The C α data were measured in dry trehalose-protected POPE/POPG (8:7) bilayers. The CO data were measured in frozen hydrated DMPC/DMPG (8:7) membranes.

Table 1: ^{13}C – ^{31}P Distances of Penetratin Residues in Lipid Membranes at a P:L Ratio of 1:15 and 233 K^a

residue	^{13}C – ^{31}P distance (Å)
Ile ₃	C α , 8.2; C $\gamma 2$, 6.9; C $\delta 1$, 6.9
Arg ₁₀	CO, 7.8; C α , 6.8; C ζ , 4.2, 6.0
Lys ₁₃	C α , 6.9; C ϵ , 4.0, 5.5

^a C α and Lys₁₃ C α distances obtained from ref 15.

Using standard geometries for β -sheets, where interstrand hydrogen bonds have $R_{\text{N-O}}$ distances of 2.8–3.4 Å and backbone torsion angles are -139° (ϕ) and 135° (ψ), we built a β -sheet model for penetratin at low temperatures that is consistent with

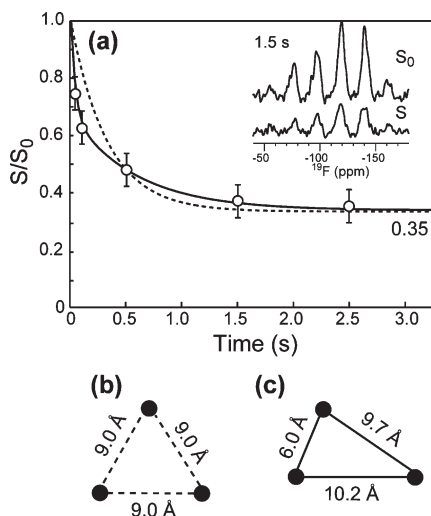


FIGURE 7: (a) Normalized CODEX intensities as a function of mixing time for 4- ^{19}F -Phe $_7$ penetratin in a trehalose-protected DMPC/DMPG (8:7) membrane. The data were collected under 8 kHz MAS and at 233 K. Representative S_0 and S spectra are shown. (b) Equilateral triangle geometry used to generate the dashed-line fit curve in panel a. (c) Three-spin geometry with unequal distances used to obtain the solid-line best-fit curve in panel a.

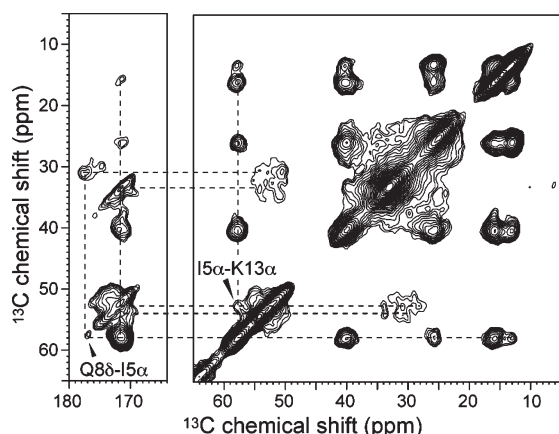


FIGURE 8: 2D ^{13}C – ^{13}C correlation spectrum of Ile $_5$ -, Gln $_8$ -, and Lys $_{13}$ -labeled penetratin in DMPC/DMPG (8:7) bilayers at 249 K. The spin diffusion mixing time was 50 ms. Two inter-residue cross-peaks were detected and assigned.

the ^{19}F and ^{13}C spin diffusion data (38, 39). Three penetratin β -strands are arranged as a trimer, with the middle strand antiparallel to the two outer strands and shifted by one residue (Figure 9a). This arrangement gives interstrand I5 α –K13 α distances of 4.2–5.8 Å, consistent with the 2D ^{13}C spectrum. The three Phe $_7$ rings point to the same side of the β -sheet, giving ^{19}F – ^{19}F distances of 6.0, 9.7, and 10 Å (Figure 9b). Short Q8 δ –I5 α distances cannot be satisfied within the same β -sheet but require two β -sheets stacked in parallel, with an intersheet distance of ~ 10 Å. This gives a Q8 δ –I5 α distance of 5.7 Å (Figure 9a), where the Q8 χ_1 angle is -177° , which is the dominant rotamer of Gln in the β -sheet conformation (40).

DISCUSSION

Interaction of Charged Side Chains in Penetratin with Lipid Phosphates. The main finding of this study is that an arginine and a lysine side chain in penetratin both form close contacts with the lipid phosphates at low temperatures.

The Arg $_{10}$ C ζ –P distance of 4.2 Å and the Lys $_{13}$ C ϵ –P distance of 4.0 Å both indicate the formation of N–H \cdots O–P hydrogen bonds. Figure 10 shows the side chain conformations of Arg $_{10}$ and Lys $_{13}$ and the spatial arrangements with a phosphate group that satisfy the distances measured here. The N–O distances in both cases must be less than 3.0 Å to satisfy the experimental distances from C ζ and C ϵ to ^{31}P .

The short distances from the Arg $_{10}$ side chain to the lipid ^{31}P indicate that guanidinium–phosphate complexation occurs not only in antimicrobial peptides but also in cell-penetrating peptides, even though they differ in whether they cause permanent membrane damage. The similarity of lipid–peptide charge–charge attraction and hydrogen bond formation suggests that penetratin, like some AMPs, also uses this interaction as the main mechanism for its function, which is crossing the lipid membrane. The fundamental driving force for formation of the complex is the reduction in the free energy when a neutral species crosses the bilayer. The complexation entails that the peptide drags some lipid headgroups into the hydrophobic region of the membrane, thus causing membrane disorder. However, since no isotropic signal was observed in the ^{31}P spectra of penetratin-containing POPC/POPG (8:7) membranes (15), the disorder is probably transient and not observable on the NMR time scale or under NMR experimental conditions. The ^{13}C – ^{31}P distances must be measured at low temperatures in the gel-phase membrane to freeze molecular motions that would average the dipolar couplings. At physiological temperature where motion is abundant and the penetratin structure is neither a canonical α -helix nor a β -strand (17), whether the ^{13}C – ^{31}P distances remain short is not possible to determine directly but can be inferred from the side chain dynamics of the residues (see below).

More interestingly, we found that Arg $_{10}$ and Lys $_{13}$ side chains both establish short distances to ^{31}P at low temperatures. This is at first puzzling, since it is well documented that CPP analogues in which arginine residues were replaced with lysine have much weaker translocation abilities (41, 42). For penetratin, which contains three arginines and four lysines, cellular uptake efficiencies have been compared among the wild-type peptide, the all-arginine analogue, and the all-lysine analogue. The efficiency was found to be the highest for the all-arginine analogue and the lowest for the all-lysine analogue (43). Since both arginine and lysine bear a positive charge at neutral pH, the higher activity of arginine-rich peptides has been suggested to be due to the more diffuse charge distribution of the guanidinium group, or the ability of guanidinium ions to form multiple hydrogen bonds with oxyanions in a spatially directed manner (44).

We propose that the similar ^{13}C – ^{31}P distances of Arg $_{10}$ and Lys $_{13}$ are true only at low temperatures at which the REDOR experiments were conducted. Low temperatures stabilize charge–charge interactions and mask different lipid interactions between Arg and Lys at physiological temperature. Indeed, there is good evidence for a much weaker interaction of the lysine side chain with phosphates at ambient temperature. First, whereas the Arg $_{10}$ N η –H η order parameters could be measured, attempts to determine the Lys $_{13}$ N ζ order parameter failed due to unstable ^1H – ^{15}N cross polarization, which in itself indicates extensive dynamics of the amino group. Second, Arg $_{10}$ C δ and N η groups have C–H and N–H order parameters of 0.42 and 0.30 ± 0.05 at 303 K, respectively, which are relatively large considering that they are three and six bonds from the backbone C α group, respectively. Further, the similar order parameters indicate that the guanidinium moiety as a whole is relatively

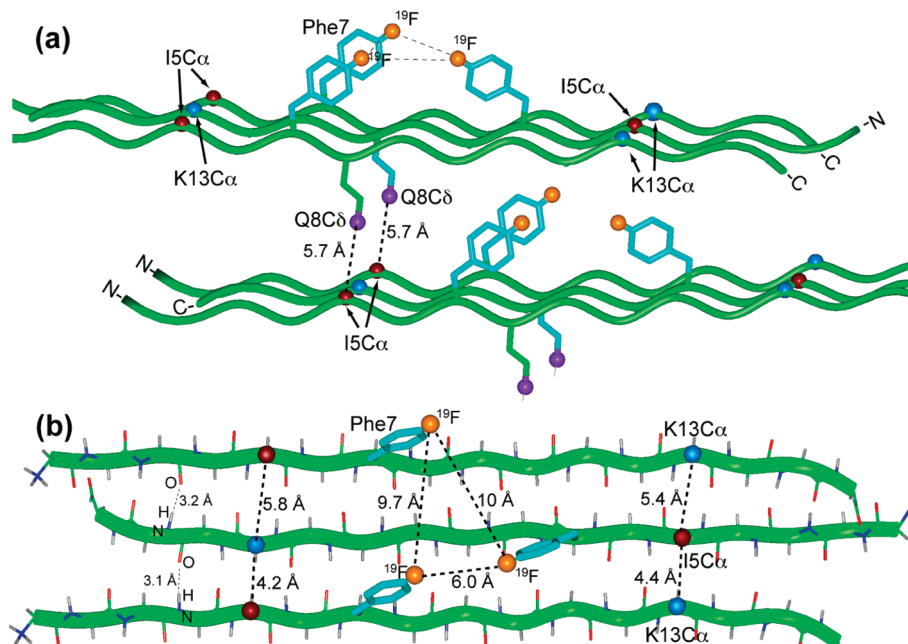


FIGURE 9: Oligomeric structure of penetratin in the gel-phase membrane: (a) side view and (b) top view. Constraints used to build the model include Phe₇ ¹⁹F–¹⁹F distances of 6.0, 9.7, and 10 Å, I5α–Q8δ and I5α–K13α distances of < 6.0 Å, *R*_{N–O} hydrogen bond distances of 2.8–3.4 Å, and intersheet distances of ~10 Å. The β-strand backbone has uniform ϕ and ψ angles of -139° and 135° , respectively. The χ_1 angle is -177° for both Phe₇ and Gln₈.

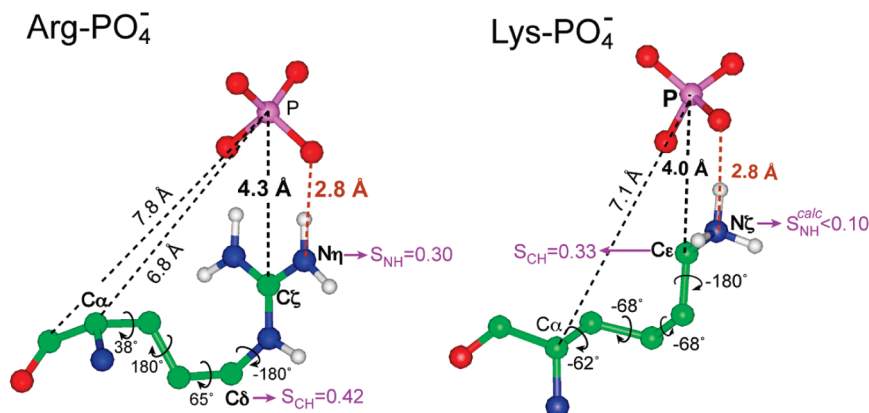


FIGURE 10: Low-temperature side chain conformation and phosphate interaction of Arg₁₀ and Lys₁₃ in penetratin. The measured ¹³C–³¹P distances are indicated in black; the implied N–H...O hydrogen bond distances are indicated in brown. Side chain torsion angles that satisfy both backbone and side chain ¹³C–³¹P distances are indicated. At physiological temperature, side chain order parameters of various segments indicate that the lysine–phosphate complex is significantly weakened whereas the arginine–phosphate complex remains.

rigid at physiological temperature, which should facilitate its complexation with the phosphate groups. In comparison, the Lys₁₃ Nζ–Hζ order parameter, although not directly measurable, can be estimated as the product of the Cε *S*_{CH} of 0.33 with an additional scaling factor of 0.33 due to the three-site jumps of the amino group. Thus, the maximum Lys₁₃ Nζ–Hζ order parameter should be only 0.10, which is much smaller than the Arg₁₀ Nη order parameter of 0.30. With this small order parameter, the Lys₁₃ amino group is unlikely to form any long-lasting hydrogen bonds with lipid phosphates.

The fact that Arg₁₀ adopts a β-sheet backbone conformation that is independent of the temperature or membrane composition, in contrast to all other residues seen so far in penetratin, further supports the unique interaction of arginine with lipid phosphates. Residues Ile₃, Ile₅, Gln₈, Asn₉, and Lys₁₃ all exhibit coil-like chemical shifts at high temperatures, which were assigned to a β-turn conformation (17). These data, together with the Arg₁₀ chemical shifts measured here, suggest that the β-turns

connect a short stretch of β-strand encompassing Arg₁₀. β-Turn residues separated by short β-strands are present in various naturally occurring proteins. For example, elastins have recurring (VPGVV)_{*n*} sequences in which the central PG residues adopt a β-turn conformation whereas the flanking Val residues have the β-strand conformation (45).

For penetratin, between the β-turn Asn₉ and Lys₁₃, there are two arginine residues and one Met (RRM). It is very likely that the conformational propensity of Arg₁₀ is not unique to this residue but is also true for Arg₁₁, because the peptide backbone may be forced into an extended structure to allow the lipid headgroups to approach the charged guanidinium moieties to form the guanidinium–phosphate complex. In other words, guanidinium–phosphate interactions may be the cause of the persistent β-sheet conformation of Arg₁₀ at high and low temperatures. As a corollary, the fact that Lys₁₃ adopts the β-turn instead of β-strand conformation at high temperatures is yet another piece of evidence that the ammonium group has

much weaker interactions with the phosphates in the liquid-crystalline membrane.

The β -sheet oligomeric structure of penetratin in the gel-phase membrane is energetically favorable. The establishment of intermolecular $\text{C}=\text{O} \cdots \text{H}-\text{N}$ hydrogen bonds reduces the free energy cost of inserting the peptide into the membrane (46). As discussed above, the extended conformation (Figure 9) may facilitate the close approach of lipid phosphate groups with the cationic side chains, thus allowing both arginine and lysine to interact with the phosphates and establish short $^{13}\text{C}-^{31}\text{P}$ distances (Figure 10).

In conclusion, we have shown that strong guanidinium-phosphate interactions exist in the cell-penetrating peptide penetratin, similar to antimicrobial peptides. Moreover, by considering not only low-temperature $^{13}\text{C}-^{31}\text{P}$ distances of Arg₁₀ and Lys₁₃ but also high-temperature order parameters of the two side chains and the unique high-temperature β -strand conformation of Arg₁₀, we deduce that the arginine side chain interacts more strongly with lipid phosphates than the lysine side chain at physiological temperature. Therefore, charge- and hydrogen bond-stabilized guanidinium-phosphate interaction not only is responsible for membrane translocation of this cationic peptide but also influences the conformation of the peptide.

ACKNOWLEDGMENT

We thank Professor Klaus Schmidt-Rohr for discussions of the ^{19}F CODEX results.

SUPPORTING INFORMATION AVAILABLE

^{13}C chemical shift assignments of Arg₁₀-labeled penetratin in POPC/POPG membranes and rmsd analyses of REDOR data. This material is available free of charge via the Internet at <http://pubs.acs.org>.

REFERENCES

- Eguchi, A., Akuta, T., Okuyama, H., Senda, T., Yokoi, H., Inokuchi, H., and Fujita, S.; et al. (2001) Protein transduction domain of HIV-1 Tat protein promotes efficient delivery of DNA into mammalian cells. *J. Biol. Chem.* 276, 26204–26210.
- Gratton, J. P., Yu, J., Griffith, J. W., Babbitt, R. W., Scotland, R. S., Hickey, R., and Giordano, F. J.; et al. (2003) Cell-permeable peptides improve cellular uptake and therapeutic gene delivery of replication-deficient viruses in cells and in vivo. *Nat. Med.* 9, 357–362.
- Schwarze, S. R., Ho, A., Vocero-Akbani, A., and Dowdy, S. F. (1999) In vivo protein transduction: Delivery of a biologically active protein into the mouse. *Science* 285, 1569–1572.
- Fischer, R., Fotin-Mleczek, M., Hufnagel, H., and Brock, R. (2005) Break on through to the other side: Biophysics and cell biology shed light on cell-penetrating peptides. *ChemBioChem* 6, 2126–2142.
- Richard, J. P., Melikov, K., Vives, E., Ramos, C., Verbeure, B., Gait, M. J., and Chernomordik, L. V.; et al. (2003) Cell-penetrating peptides. A reevaluation of the mechanism of cellular uptake. *J. Biol. Chem.* 278, 585–590.
- Derossi, D., Calvet, S., Trembleau, A., Brunissen, A., Chassaing, G., and Prochiantz, A. (1996) Cell internalization of the third helix of the Antennapedia homeodomain is receptor-independent. *J. Biol. Chem.* 271, 18188–18193.
- Berlose, J. P., Convert, O., Derossi, D., Brunissen, A., and Chassaing, G. (1996) Conformational and associative behaviours of the third helix of antennapedia homeodomain in membrane-mimetic environments. *Eur. J. Biochem.* 242, 372–386.
- Prochiantz, A. (1996) Getting hydrophilic compounds into cells: Lessons from homeopeptides. *Curr. Opin. Neurobiol.* 6, 629–634.
- Binder, H., and Lindblom, G. (2003) Charge-dependent translocation of the Trojan peptide penetratin across lipid membranes. *Biophys. J.* 85, 982–995.
- Drin, G., Cottin, S., Blanc, E., Rees, A. R., and Temsamani, J. (2003) Studies on the internalization mechanism of cationic cell-penetrating peptides. *J. Biol. Chem.* 278, 31192–31201.
- Zhang, W., and Smith, S. O. (2005) Mechanism of penetration of Antp(43–58) into membrane bilayers. *Biochemistry* 44, 10110–10118.
- Rothbard, J. B., Jessop, T. C., Lewis, R. S., Murray, B. A., and Wender, P. A. (2004) Role of membrane potential and hydrogen bonding in the mechanism of translocation of guanidinium-rich peptides into cells. *J. Am. Chem. Soc.* 126, 9506–9507.
- Herce, H. D., and Garcia, A. E. (2007) Molecular dynamics simulations suggest a mechanism for translocation of the HIV-1 TAT peptide across lipid membranes. *Proc. Natl. Acad. Sci. U.S.A.* 104, 20805–20810.
- Derossi, D., Joliot, A. H., Chassaing, G., and Prochiantz, A. (1994) The third helix of the Antennapedia homeodomain translocates through biological membranes. *J. Biol. Chem.* 269, 10444–10450.
- Su, Y., Mani, R., and Hong, M. (2008) Asymmetric insertion of membrane proteins in lipid bilayers by solid-state NMR paramagnetic relaxation enhancement: A cell-penetrating peptide example. *J. Am. Chem. Soc.* 130, 8856–8864.
- Buffy, J. J., Hong, T., Yamaguchi, S., Waring, A., Lehrer, R. I., and Hong, M. (2003) Solid-State NMR Investigation of the Depth of Insertion of Protegrin-1 in Lipid Bilayers Using Paramagnetic Mn^{2+} . *Biophys. J.* 85, 2363–2373.
- Su, Y., Mani, R., Doherty, T., Waring, A. J., and Hong, M. (2008) Reversible sheet-turn conformational change of a cell-penetrating peptide in lipid bilayers studied by solid-state NMR. *J. Mol. Biol.* 381, 1133–1144.
- Tang, M., Waring, A. J., and Hong, M. (2007) Phosphate-mediated arginine insertion into lipid membranes and pore formation by a cationic membrane peptide from solid-state NMR. *J. Am. Chem. Soc.* 129, 11438–11446.
- Tang, M., Waring, A. J., Lehrer, R. I., and Hong, M. (2008) Effects of guanidinium-phosphate hydrogen bonding on the membrane-bound structure and activity of an arginine-rich membrane peptide from solid-state NMR spectroscopy. *Angew. Chem., Int. Ed.* 47, 3202–3205.
- Yamaguchi, S., Hong, T., Waring, A., Lehrer, R. I., and Hong, M. (2002) Solid-state NMR investigations of peptide-lipid interaction and orientation of a β -sheet antimicrobial peptide, protegrin. *Biochemistry* 41, 9852–9862.
- Tang, M., Waring, A. J., and Hong, M. (2007) Trehalose-protected lipid membranes for determining membrane protein structure and insertion. *J. Magn. Reson.* 184, 222–227.
- Crowe, J. H., Carpenter, J. F., and Crowe, L. M. (1998) The role of vitrification in anhydrobiosis. *Annu. Rev. Physiol.* 60, 73–103.
- Takegoshi, K., Nakamura, S., and Terao, T. (2001) C-13-H-1 dipolar-assisted rotational resonance in magic-angle spinning NMR. *Chem. Phys. Lett.* 344, 631–637.
- Munowitz, M. G., Griffin, R. G., Bodenhausen, G., and Huang, T. H. (1981) Two-dimensional rotational spin-echo nuclear magnetic resonance in solids: Correlation of chemical shift and dipolar interactions. *J. Am. Chem. Soc.* 103, 2529–2533.
- Hong, M., Gross, J. D., Rienstra, C. M., Griffin, R. G., Kumashiro, K. K., and Schmidt-Rohr, K. (1997) Coupling amplification in 2D MAS NMR and its application to torsion angle determination in peptides. *J. Magn. Reson.* 129, 85–92.
- Rhim, W. K., Elleman, D. D., and Vaughan, R. W. (1973) Analysis of multiple-pulse NMR in solids. *J. Chem. Phys.* 59, 3740–3749.
- Jaroniec, C. P., Tounge, B. A., Rienstra, C. M., Herzfeld, J., and Griffin, R. G. (1999) Measurement of $^{13}\text{C}-^{15}\text{N}$ distances in uniformly ^{13}C labeled biomolecules: J-decoupled REDOR. *J. Am. Chem. Soc.* 121, 10237–10238.
- Jaroniec, C. P., Tounge, B. A., Herzfeld, J., and Griffin, R. G. (2001) Frequency selective heteronuclear dipolar recoupling in rotating solids: Accurate $^{13}\text{C}-^{15}\text{N}$ distance measurements in uniformly $^{13}\text{C}, ^{15}\text{N}$ -labeled peptides. *J. Am. Chem. Soc.* 123, 3507–3519.
- Hohwy, M., Rienstra, C. M., Jaroniec, C. P., and Griffin, R. G. (1999) Fivefold symmetric homonuclear dipolar recoupling in rotating solids: Application to double-quantum spectroscopy. *J. Chem. Phys.* 110, 7983–7992.
- deAzevedo, E. R., Bonagamba, T. J., Hu, W., and Schmidt-Rohr, K. (1999) Centerband-only detection of exchange: Efficient analysis of dynamics in solids by NMR. *J. Am. Chem. Soc.* 121, 8411–8412.
- Buffy, J. J., Waring, A. J., and Hong, M. (2005) Determination of Peptide Oligomerization in Lipid Membranes with Magic-Angle Spinning Spin Diffusion NMR. *J. Am. Chem. Soc.* 127, 4477–4483.
- Luo, W., and Hong, M. (2006) Determination of the oligomeric number and intermolecular distances of membrane protein assemblies

- by anisotropic ^1H -driven spin diffusion NMR spectroscopy. *J. Am. Chem. Soc.* 128, 7242–7251.
33. Zhang, H., Neal, S., and Wishart, D. S. (2003) RefDB: A database of uniformly referenced protein chemical shifts. *J. Biomol. NMR* 25, 173–195.
34. Cady, S. D., and Hong, M. (2008) Amantadine-Induced Conformational and Dynamical Changes of the Influenza M2 Transmembrane Proton Channel. *Proc. Natl. Acad. Sci. U.S.A.* 105, 1483–1488.
35. Tang, M., Waring, A. J., and Hong, M. (2008) Arginine Dynamics in a Membrane-Bound Cationic β -Hairpin Peptide from Solid-State NMR. *ChemBioChem* 9, 1487–1492.
36. Buffy, J. J., Waring, A. J., Lehrer, R. I., and Hong, M. (2003) Immobilization and aggregation of the antimicrobial peptide protegrin-1 in lipid bilayers investigated by solid-state NMR. *Biochemistry* 42, 13725–13734.
37. Huster, D., Xiao, L. S., and Hong, M. (2001) Solid-state NMR investigation of the dynamics of colicin Ia channel-forming domain. *Biochemistry* 40, 7662–7674.
38. Mani, R., Cady, S. D., Tang, M., Waring, A. J., Lehrer, R. I., and Hong, M. (2006) Membrane-dependent oligomeric structure and pore formation of a β -hairpin antimicrobial peptide in lipid bilayers from solid-state NMR. *Proc. Natl. Acad. Sci. U.S.A.* 103, 16242–16247.
39. Mani, R., Tang, M., Wu, X., Buffy, J. J., Waring, A. J., Sherman, M. A., and Hong, M. (2006) Membrane-bound dimer structure of a β -hairpin antimicrobial peptide from rotational-echo double-resonance solid-state NMR. *Biochemistry* 45, 8341–8349.
40. Lovell, S. C., Word, J. M., Richardson, J. S., and Richardson, D. C. (2000) The penultimate rotamer library. *Proteins: Struct., Funct., Genet.* 40, 389–408.
41. Wender, P. A., Mitchell, D. J., Pattabiraman, K., Pelkey, E. T., Steinman, L., and Rothbard, J. B. (2000) The design, synthesis, and evaluation of molecules that enable or enhance cellular uptake: Peptoid molecular transporters. *Proc. Natl. Acad. Sci. U.S.A.* 97, 13003–13008.
42. Mitchell, D. J., Kim, D. T., Steinman, L., Fathman, C. G., and Rothbard, J. B. (2000) Polyarginine enters cells more efficiently than other polycationic homopolymers. *J. Pept. Res.* 56, 318–325.
43. Amand, H. L., Fant, K., Nordén, B., and Esbjörner, E. K. (2008) Stimulated endocytosis in penetratin uptake: Effect of arginine and lysine. *Biochem. Biophys. Res. Commun.* 371, 621–625.
44. Jiang, Y., Ruta, V., Chen, J., Lee, A., and MacKinnon, R. (2003) The principle of gating charge movement in a voltage-dependent K^+ channel. *Nature* 423, 42–48.
45. Yao, X. L., and Hong, M. (2004) Structural Distribution in an Elastin-Mimetic Peptide (VPGVG) $_3$ Investigated by Solid-State NMR. *J. Am. Chem. Soc.* 126, 4199–4210.
46. White, S. H., and Wimley, W. C. (1999) Membrane protein folding and stability: Physical principles. *Annu. Rev. Biophys. Biomol. Struct.* 28, 319–365.